

Inhibition of CorA-Dependent Magnesium Homeostasis Is Cidal in *Mycobacterium tuberculosis*

Yumi Park,^{a*} Yong-Mo Ahn,^{a*} Surendranadha Jonnala,^a Sangmi Oh,^a Julia M. Fisher,^a Michael B. Goodwin,^a Thomas R. Ioerger,^b Laura E. Via,^a Tracy Bayliss,^c Simon R. Green,^c Peter C. Ray,^c Paul G. Wyatt,^c Clifton E. Barry III,^a Helena I. Boshoff^a

^aTuberculosis Research Section, Laboratory of Clinical Immunology and Microbiology, National Institute of Allergy and Infectious Disease, National Institutes of Health, Bethesda, Maryland, USA

^bDepartment of Computer Science and Engineering, Texas A&M University, College Station, Texas, USA

^cDrug Discovery Unit, Division of Biological Chemistry and Drug Discovery, School of Life Sciences, University of Dundee, Dundee, United Kingdom

ABSTRACT Mechanisms of magnesium homeostasis in *Mycobacterium tuberculosis* are poorly understood. Here, we describe the characterization of a pyrimidinetrione amide scaffold that disrupts magnesium homeostasis in the pathogen by direct binding to the CorA Mg²⁺/Co²⁺ transporter. Mutations in domains of CorA that are predicted to regulate the pore opening in response to Mg²⁺ ions conferred resistance to this scaffold. The pyrimidinetrione amides were cidal against the pathogen under both actively replicating and nonreplicating conditions *in vitro* and were efficacious against the organism during macrophage infection. However, the compound lacked efficacy in infected mice, possibly due to limited exposure. Our results indicate that inhibition of Mg²⁺ homeostasis by CorA is an attractive target for tuberculosis drug discovery and encourage identification of improved CorA inhibitors.

KEYWORDS CorA transporter, *Mycobacterium tuberculosis*, magnesium homeostasis, pyrimidinetrione amide, structure-activity relationship

Short-course chemotherapy for tuberculosis was adopted by the WHO in 1991 for drug-sensitive disease, requiring 6 months of multidrug treatment (1). The risk of drug-related toxicity, as well as noncompliance, increases proportionally over time, which has motivated efforts to reduce the treatment duration (2). The current front-line drug regimen consists of drugs that target RNA synthesis (rifampin) and cell wall biosynthesis (isoniazid/ethambutol) and pyrazinamide (which has an ill-defined mechanism of action) (3, 4). Identification of drugs that target novel pathways in the pathogen has been proposed as a way of developing new drug combinations that could reduce treatment duration (5). To this end, mechanisms that are critical for survival under various growth conditions are predicted to encompass targets that could lead to a rapid decline in bacterial viability *in vivo*.

Magnesium is an essential cofactor in a plethora of enzymatic reactions. It plays a structural role in the integrity of nucleic acids and proteins, as well as maintaining the integrity of the cell membrane and cell wall (6, 7). In *M. tuberculosis*, three mutants that exhibited attenuation at low extracellular magnesium concentrations have been described: *perM*, encoding a membrane protein of unknown function, deletion of which results in *in vivo* attenuation and inability to grow at low Mg²⁺ concentrations; *phoP*, encoding the transcriptional regulator of a two-component system important for complex lipid biosynthesis and virulence; and *mgtC*, which encodes a P-type ATPase likely acting as an accessory protein for Mg²⁺ import, deletion of which results in inability to grow at low Mg²⁺ concentrations at acidic pH and in loss of virulence (8–10). The *in vivo* attenuation of these mutants in *M. tuberculosis*, as well as other

Citation Park Y, Ahn Y-M, Jonnala S, Oh S, Fisher JM, Goodwin MB, Ioerger TR, Via LE, Bayliss T, Green SR, Ray PC, Wyatt PG, Barry CE, III, Boshoff HI. 2019. Inhibition of CorA-dependent magnesium homeostasis is cidal in *Mycobacterium tuberculosis*. *Antimicrob Agents Chemother* 63:e01006-19. <https://doi.org/10.1128/AAC.01006-19>.

Copyright © 2019 American Society for Microbiology. All Rights Reserved.

Address correspondence to Helena I. Boshoff, hboshoff@niaid.nih.gov.

* Present address: Yumi Park, Center for Personalized Precision Medicine of TB, Inje University College of Medicine, Busan, Republic of Korea; Yong-Mo Ahn, Department of Pharmacology, Physiology and Neuroscience, New Jersey Medical School, Rutgers, The State University of New Jersey, Newark, New Jersey, USA.

Y.P. and Y.-M.A. contributed equally to this work.

Received 14 May 2019

Returned for modification 2 June 2019

Accepted 2 August 2019

Accepted manuscript posted online 5 August 2019

Published 23 September 2019

bacterial pathogens with inactivated Mg^{2+} -dependent processes, has been hypothesized to point to restriction of this essential cation as a possibly host-mediated mechanism to control bacterial pathogens (7–10). Indeed, phagosomal Mg^{2+} concentrations, at least during *Salmonella enterica* serovar Typhimurium infection, have been estimated to be in the 10 to 50 μM range (11). The predicted low phagosomal Mg^{2+} concentrations and the increased Mg^{2+} requirement of *M. tuberculosis* at low pH suggest that access to the nutrient could be growth limiting *in vivo*. Consequently, inhibitors of Mg^{2+} homeostasis would affect bacterial survival at every stage of host pathogenesis (12). The mechanisms by which *M. tuberculosis* maintains Mg^{2+} homeostasis are poorly understood. *M. tuberculosis* encodes two Mg^{2+} transporters, CorA and MgtE, neither of which is apparently essential based on saturating genome transposon mutagenesis studies (13, 14).

In this work, we describe the identification of a series of compounds that exert potent growth inhibition on *M. tuberculosis* and inhibit Mg^{2+} uptake via direct binding to the CorA transporter. A representative of this inhibitor series lacked *in vivo* efficacy against *M. tuberculosis* in mice. This was presumed to be related to insufficient compound exposure *in vivo*.

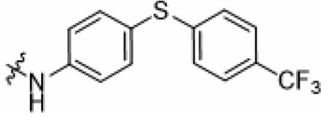
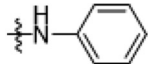
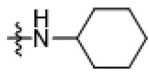

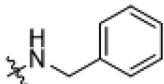
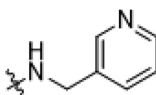
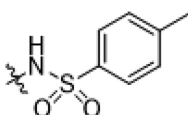
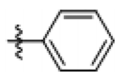
RESULTS

Identification of a pyrimidinetrione amide with Gram-positive antibacterial activity. The series, as represented by compound 1, was identified in a large whole-cell phenotypic screen against *M. tuberculosis* and was found to have potent antimycobacterial activity on two distinct growth media (Table 1). The pyrimidinetrione amide core is based on barbituric acid. In order to establish some preliminary structure-activity relationship (SAR), analogues were prepared with different amines, including a simple aniline (compound 2), cyclohexylamine (compound 3), butylamine (compound 4), benzylamine (compound 5), and 3-picolylamine (compound 6). Except for compound 2, none showed equivalent antimicrobial activities in both media (Table 1). Although compound 5 showed good potency in glycerol-alanine salts-Tween 80 (GAST) medium (a minimal medium lacking bovine serum albumin [BSA]), the lack of potency in 7H9 medium suggested high protein binding, discouraging further evaluation. The modification of the amide linker to generate either a sulfonylamine (compound 7) or a ketone (compound 8) also resulted in complete loss of antitubercular activity.

Based on the initial SAR described in Table 1, a series of compounds modified in the aniline moiety were further evaluated (Table 2). Interestingly, irrespective of the substituents in the *para* position of the aniline, compounds 9 to 14 showed good antitubercular activities. Compounds 15 and 16, which had a substituent in the *ortho* position, also showed activity, while other analogues with heteroaromatic rings instead of phenyl groups, such as pyridine (compounds 17 to 19) and isoxazole (compound 20), generally had reduced potency. Because the core is related to barbituric acid, we wanted to rule out nonspecific effects due to mitochondrial-membrane depolarization (15). We tested for cytotoxicity against HepG2 cells during growth on either glucose or galactose as a sole carbon source. Growth on galactose forces cells to use mitochondrial respiration to generate ATP rather than through glycolysis, as occurs during growth on glucose (16). This showed that several of the compounds were associated with clear mitochondrial toxicity, as evidenced by the enhanced cytotoxicity of compounds during growth on galactose. Cytotoxicity in galactose medium generally tracked with antimycobacterial potency (see Fig. S1 in the supplemental material). However, compounds having electron-donating alkyl groups, methyl (compound 9) and isopropyl (compound 10), were both selective and had no mitochondrial toxicity based on a lack of inhibition of HepG2 cell growth on either glucose or galactose.

The compound series was not selectively antitubercular, as seen from its broader-spectrum activity against *Mycobacterium smegmatis*, *Bacillus subtilis*, and *Staphylococcus aureus* (see Table S1 in the supplemental material). However, the series lacked activity against Gram-negative bacteria, such as *Escherichia coli* and *Pseudomonas aeruginosa* (data not shown), suggesting a mechanism of action unique to Gram-positive bacteria.

TABLE 1 Antitubercular activities of pyrimidinetrione amide analogues

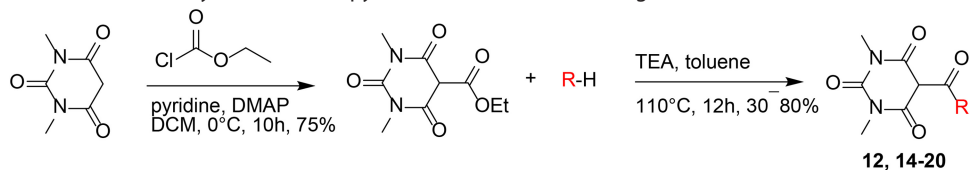
Compound ^a	Chemical structure R	MIC (μM) ^b	
		7H9	GAST
1		0.2	0.29
2		2.24	1.49
3		>50	9.4
4		25	12.5
5		50	0.39
6		>50	>50
7		>50	37
8		>50	>50

^aCompounds 1 to 8 are all known molecules.

^bMIC of compound against *M. tuberculosis* H37Rv in Middlebrook 7H9-BSA containing glucose/glycerol/Tween 80 (7H9) or GAS medium with Tween 80 (GAST).

The pyrimidinetrione amide inhibits magnesium uptake in *M. tuberculosis*. In an effort to understand the mechanism of action of the series, mutants resistant to compound 1 were raised. Mutants were obtained at a frequency of resistance of 10^{-8} . Three that were confirmed to be more than 100-fold resistant to the compound were submitted for whole-genome sequencing. Two had independent mutations in *corA* (*Rv1239c*), *corA*::E212D, and *corA*::A317S; other single nucleotide polymorphisms (SNPs) present showed no evidence of mechanism-of-action-associated resistance (Table 3). The third mutant had an SNP profile identical to that of the second mutant, suggesting that it may have arisen as a sibling.

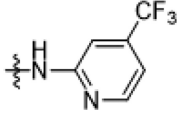
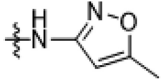
The *corA* gene encodes a putative magnesium and cobalt transporter predicted to be nonessential by genome-wide transposon mutagenesis studies (13, 14). To confirm that SNPs in *corA* were associated with resistance, we raised strains resistant to compounds 1, 10, 12, 13, and 15 and specifically sequenced their *corA* genes. All the resistant strains contained point mutations within the *corA* gene (see Table S2 in the supplemental material). To interpret the effects of these mutations on *corA* function, an

TABLE 2 Antitubercular activities and cytotoxicities of pyrimidinetrione amide analogues

Compound ^a	Chemical structure R	MIC (μM) ^b				Cytotoxicity (IC ₅₀ [μM]) ^c	
		7H9	GAST	Butyrate	7H9 (<i>corA::E212D</i>)	Glucose	Galactose
1		0.20	0.29	0.10	>50	29.5	5.50
2		2.24	1.49	ND ^d	ND	ND	ND
9		1.20	0.78	1.56	>50	>100	>100
10		0.59	0.20	3.13	6.25	>100	>100
11		3.10	1.56	3.13	3.10	72.5	23.0
12		0.78	0.20	0.59	6.25	26.6	3.50
13		0.20	0.07	1.17	3.13	24.6	3.80
14		3.10	4.69	3.13	25.0	8.54	2.10
15		0.78	0.20	1.17	9.38	19.0	5.20
16		6.30	1.17	6.25	>50	>100	50
17		4.70	3.13	3.13	>50	>100	28.0
18		>50	>50	>50	>50	ND	ND

(Continued on following page)

TABLE 2 (Continued)

Compound ^a	Chemical structure R	MIC (μ M) ^b				Cytotoxicity (IC ₅₀ [μ M]) ^c	
		7H9	GAST	Butyrate	7H9 (<i>corA</i> ::E212D)	Glucose	Galactose
19		>50	>50	>50	>50	ND	ND
20		9.38	2.34	50	>50	ND	ND

^aCompounds 1, 2, 9 to 11, and 13 are known molecules.

^bMICs of compounds against *M. tuberculosis* H37Rv in Middlebrook 7H9-BSA containing glucose/glycerol/Tween 80 (7H9), GAS medium with Tween 80 (GAST), Middlebrook 7H9-BSA-tyloxapol-butyrates-0.1 mM nitrite, pH 6.0 (Butyrate), and a *CorA*-E212D mutant *M. tuberculosis* strain in Middlebrook 7H9-BSA containing glucose-glycerol-Tween 80 [7H9 (*corA*::E212D)].

^cCytotoxicities of compounds tested against HepG2 cells in DMEM-10% FBS supplemented with glucose or galactose.

^dND, not done.

M. tuberculosis CorA (MtCorA) homology model was generated from the crystal structure of *Thermotoga maritima* CorA (TmCorA) using Phyre2 (17). Unexpectedly, the mutations did not occur at the divalent-cation sensor region, where Mg²⁺ ions bind. Instead, the homology model predicted that the mutations occurred within the acidic (E212D) and kink (G299S and M300V/L) regions, which are involved in the gating motion of CorA, and the hydrophobic tunnel (A317S), through which Mg²⁺ ions flow (see Fig. S2 in the supplemental material). The mutation data suggested that the pyrimidinetrione amide scaffold affected the gating mechanism of CorA, resulting in the inhibition of Mg²⁺ uptake (see Fig. S2). This hypothesis was supported by the Mg²⁺ dependence of the growth inhibition in *M. tuberculosis* (Fig. 1A), as well as other Gram-positive bacteria (see Table S2).

Co²⁺ was unable to rescue cells from pyrimidinetrione-dependent growth inhibition (Fig. 1B). The inability of Co²⁺ to rescue growth inhibition was not surprising, since there are no known essential cobalt-dependent enzymes in *M. tuberculosis*. Magnesium is an essential metal cofactor in many key metabolic enzymes, and the specificity of some of the pyrimidinetrione amides for inhibiting bacterial growth and not HepG2 cell growth suggested that magnesium uptake could be a novel target for drug development.

To confirm that the series inhibited Mg²⁺ uptake, intracellular concentrations of the cation were measured by inductively coupled plasma mass spectrometry (ICP-MS). This analysis confirmed that compound 10 treatment generated a concentration-dependent decrease in intracellular magnesium levels (Fig. 1C). Moxifloxacin was chosen as a negative control because it was not expected to affect cell wall or membrane integrity, both of which could potentially influence intracellular Mg²⁺ levels. However, moxifloxacin resulted in an unexpected increase in intracellular magnesium concentrations (Fig. 1C) for reasons that were not clear.

The pyrimidinetrione amide-Mg²⁺ complex binds to the CorA transporter. The core of the series shows structural similarity to the pyrimidinedione scaffold associated with Mg²⁺ binding in drugs such as raltegravir (18). To explore whether this series

TABLE 3 Mutations identified in pyrimidinetrione amide-resistant *M. tuberculosis* strains

Strain	Polymorphisms ^a
E2.1	<i>corA</i> ::E212D, 4221182::T → C (30 bp upstream of <i>Rv3776</i>)
E2.2	<i>corA</i> ::A317S, <i>Rv0275c</i> ::S233S, 3281706 → G (in aa 342/2111 of <i>mas</i>)
E2.6	Same as E2.2

^aaa, amino acids.

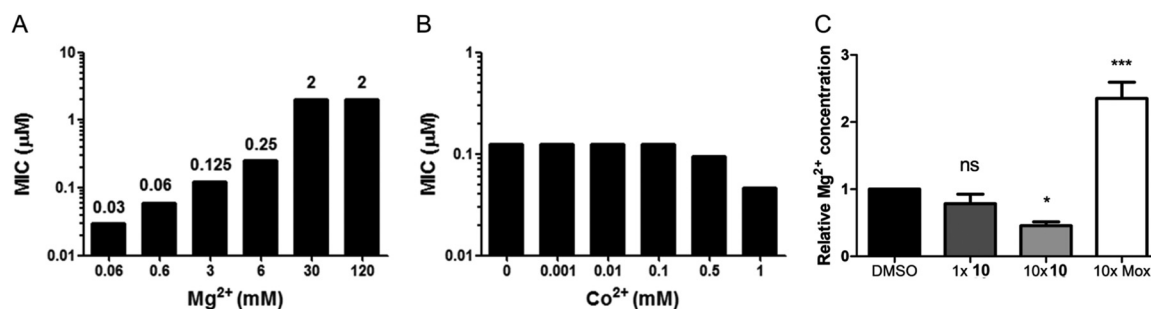


FIG 1 The pyrimidinetrione amide scaffold inhibits Mg²⁺ uptake by *M. tuberculosis*. (A) Magnesium dependence of the pyrimidinetrione amide MIC against *M. tuberculosis* in Mg²⁺-free medium with the indicated concentrations of Mg²⁺. (B) Co²⁺ dependence of the pyrimidinetrione amide MIC against *M. tuberculosis* in Co²⁺-free medium with the indicated concentrations of Co²⁺. (C) Fold changes in intracellular Mg²⁺ concentrations as measured by ICP-MS compared to vehicle (DMSO) control after 24 h of treatment with moxifloxacin (Mox) or compound 10 at 1- or 10-fold the MIC in 7H9 medium that contained 0.4 mM Mg²⁺. Significance between groups was determined by Tukey's multiple-comparison test, with significance set at *P* values of less than 0.05. *, 0.02; ***, 0.0006; ns, not significant. The error bars indicate standard deviation.

bound Mg²⁺ ions, we analyzed the UV-visible (Vis) spectral response of compound 10 upon titration with Mg²⁺ ions. A clear cation-dependent decrease in absorbance at 280 nm was seen (see Fig. S3 in the supplemental material). The coordination complex of compound 10 with Mg²⁺ was further investigated by nuclear magnetic resonance (NMR) studies; based on the splitting pattern of the signals of the asymmetric pyrimidinetrione moiety, compound 10 forms the enol tautomer when interacting with Mg²⁺ (see Fig. S4 in the supplemental material). The coordination of Mg²⁺ by this scaffold could suggest that the compounds merely act to deplete free Mg²⁺ ions, with the *corA* mutations conferring higher affinity for the Mg²⁺·6H₂O complex. However, arguing against this notion, in the absence of compound the *corA* mutants required a 250-fold higher Mg²⁺ concentration than the wild-type strain in order to grow (see Table S3 in the supplemental material).

In order to test whether the Mg²⁺-pyrimidinetrione amide complex directly bound to CorA, we determined the thermal stability of recombinantly expressed CorA in the presence of Mg²⁺ and compound 10 (Fig. 2). This showed that all these ligands increased the thermal stability of the protein, indicating binding to the transporter (Fig. 2 and Table 4). The apparent dissociation constant of CorA with metal ions and compound 10 was determined using fluorescence change based on tryptophan quenching (Table 5; see Fig. S5 in the supplemental material). The results indicated that Co²⁺ was poorly

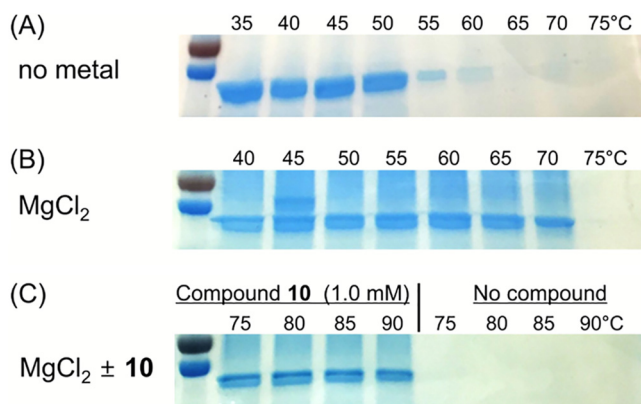


FIG 2 Magnesium and the pyrimidinetrione scaffold bind to the CorA transporter protein. The thermostability of recombinantly expressed CorA from *M. tuberculosis* was measured with no ligand (A), 0.125 mM MgCl₂ (B), and 0.125 mM MgCl₂ with or without 1.0 mM compound 10 (C). The protein was preincubated at room temperature with the indicated ligands before heating to the indicated temperatures in a thermocycler. Protein precipitates were removed by filtration, and soluble protein was analyzed by SDS-PAGE.

TABLE 4 Thermostability of CorA in the presence of metal cations, EDTA, and compound 10

CorA additive	Melting temp (°C)
None	55
0.125 mM MgCl ₂	70
1 mM compound 10	≥95
1 mM compound 10/0.125 mM MgCl ₂	≥95
1 mM EDTA/0.125 mM MgCl ₂	≥95

bound to CorA compared to Mg²⁺, whereas compound 10 bound with 2-fold higher affinity than Mg²⁺ alone, irrespective of the presence of Mg²⁺. Although this result showed that the Mg²⁺-pyrimidinetrione amide complex bound and stabilized the CorA structure, it was still unclear how this event affected intracellular Mg²⁺ homeostasis, resulting in bactericidal activity. We predicted that mutant strains, such as the *corA::E212D* strain, could survive exposure to compound 10 as a result of lower binding affinity of the CorA::E212D protein to the Mg²⁺-compound 10 complex, thereby overcoming the disruption of Mg²⁺ homeostasis. Therefore, we performed similar thermal-stability assays and fluorescence shift assays using one of the mutant CorA proteins, the purified recombinant CorA::E212D, in the presence of Mg²⁺, compound 10, or compound 10 with Mg²⁺. The assay result showed that the Mg²⁺-pyrimidinetrione amide complex could also bind to the mutated CorA::E212D (see Tables S4 and S5 in the supplemental material). This result suggested that the mutations observed on CorA do not have a measurable effect on the binding affinity of the Mg²⁺-pyrimidinetrione amide complex for the transporter (bearing in mind the limited analytical sensitivity of these assays).

Pyrimidinetrione amide decreases *M. tuberculosis* viability *in vitro* and *ex vivo* but lacks apparent *in vivo* efficacy. The pyrimidinetrione amide compound 10 was cidal against actively growing *M. tuberculosis* cells, showing a 2-log-unit kill over a week of exposure, even at concentrations as low as 2 times the MIC value. Higher concentrations resulted in a more rapid cidal effect with no detectable viable cells remaining, as determined by colony counts on solid agar (Fig. 3A). We next sought to investigate the importance of Mg²⁺ uptake under nonreplicating conditions using nonreplicating persistence induced by adaptation to hypoxia with subsequent exposure of cells to compounds under anaerobic conditions. This showed that Mg²⁺ uptake was critical under these conditions, as evidenced by the greater than 3-log-unit kill after a week of compound exposure (Fig. 3B).

The cidal consequence of disrupting Mg²⁺ homeostasis during active growth, as well as nonreplicating persistence, prompted us to explore the antitubercular effect during parasitism of host macrophages. We selected compounds that had no general cytotoxic or mitochondrial toxic effect (compounds 9 and 10); no general cytotoxic effect yet with limited mitochondrial toxicity, giving a 10-fold selectivity window (compound 16); or limited general cytotoxicity and higher mitochondrial toxicity that still gave us a greater than 10-fold selectivity window (compound 1) (Table 1). All of these compounds exerted time- and dose-dependent intracellular (*ex vivo*) killing of *M. tuberculosis* growing in macrophages (Fig. 3C).

The promising activity of compound 10 against *M. tuberculosis* during growth in macrophages encouraged us to explore its *in vivo* efficacy. Preliminary pharmacokinetic (PK) analysis indicated the half-life of compound 10 was 2.5 ± 0.4 h when dosed once daily, showing that at least twice-per-day (BID) dosing was needed. Unfortunately, the

TABLE 5 $K_d(\text{app})$ of CorA with metal cations and compound 10

CorA additive in fluorescence shift assay	$K_d(\text{app})$ (μM)
Mg ²⁺	47.5 ± 3.0
Co ²⁺	205 ± 18
Compound 10	20.0 ± 4.3
Compound 10/1 mM Mg ²⁺	24.1 ± 6.3
Compound 10/1 mM Co ²⁺	21.8 ± 4.1

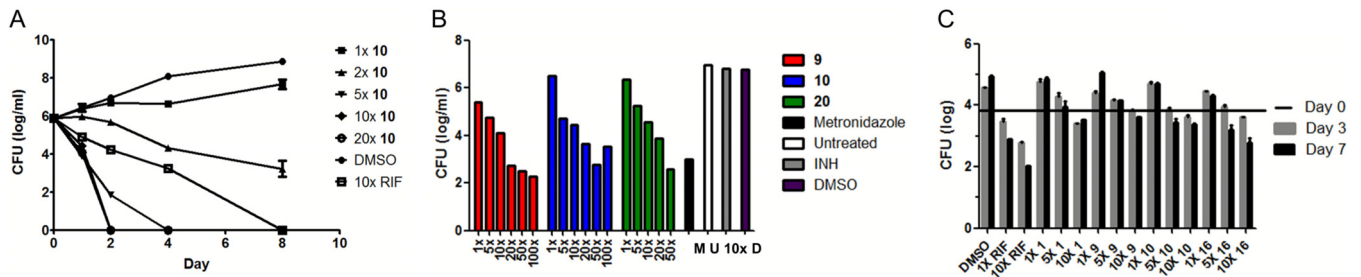


FIG 3 The pyrimidinetrione amide scaffold is cidal against replicating, as well as nonreplicating, *M. tuberculosis* *in vitro* and *ex vivo*. (A) Kill kinetics of compound 10 against *M. tuberculosis* during active replication *in vitro* compared to negative (DMSO) and positive (5 μg/ml rifampin [RIF]) controls. (B) Anaerobic cidal activities of compounds 9, 10, and 20 compared to negative (untreated, DMSO, and 1 μg/ml isoniazid [INH]) and positive (100 μM metronidazole) controls after 7 days of compound exposure. M, metronidazole; U, untreated (control); D, DMSO; 10×, 10-fold MIC concentration isoniazid. (C) Efficacies of compounds 1, 9, 10, and 16 during growth of *M. tuberculosis* in J774 macrophages compared to the negative (DMSO) and positive (0.5 and 5 μg/ml RIF) controls. The horizontal bar indicates inoculum (day 0). The error bars indicate SD.

compound was not tolerable by mice at high (100 mg/kg of body weight) doses. At 30 mg/kg, dosed BID by oral gavage, the compound achieved an area under the concentration-time curve (AUC) of 56 μg · h/ml, which gave an AUC/MIC ratio of 250 and plasma concentrations that were almost 10-fold above MICs at the first trough and just above the MIC at 24 h (0.3 μg/ml ± 0.16 [standard deviation {SD}]) (Fig. 4A). This dosing schedule was tolerable in naive mice. Subsequently, *M. tuberculosis*-infected mice were treated with 30 or 15 mg/kg BID; however, after multiple BID doses, 30 mg/kg was intolerable for the infected mice, necessitating a de-escalation to 30 mg/kg once per day for that group for the remaining dosing period. Due to adverse effects, compound 10 could not be administered at higher concentrations, and at the highest tolerable concentration, it lacked efficacy after 2 and 4 weeks of treatment in infected mouse lungs (Fig. 4B) and spleens (results not shown).

DISCUSSION

We have identified a pyrimidinetrione amide scaffold with potent *in vitro* activity against *M. tuberculosis*. Resistant mutants mapped to the CorA transporter, with Mg²⁺ supplementation abrogating the growth inhibition in a concentration-dependent fashion. Using thermostability assays and fluorescence shift assays, we were able to demonstrate that the inhibitor binds to CorA in the presence and absence of Mg²⁺. The ligand binding site for the inhibitor remains to be identified, but we were also able to show that resistance-conferring amino acid mutations had no effect on ligand binding. Instead, the mutations mapped to the acidic and kink regions of the cytoplasmic domain of the CorA transporter, which are involved in the gating motion of the pore, indicating that modes of resistance were not due to changes in CorA-ligand interaction but likely the results of perturbation of the gating motion in response to Mg²⁺ dissociation from the protein. Low cytosolic Mg²⁺ concentrations result in cation

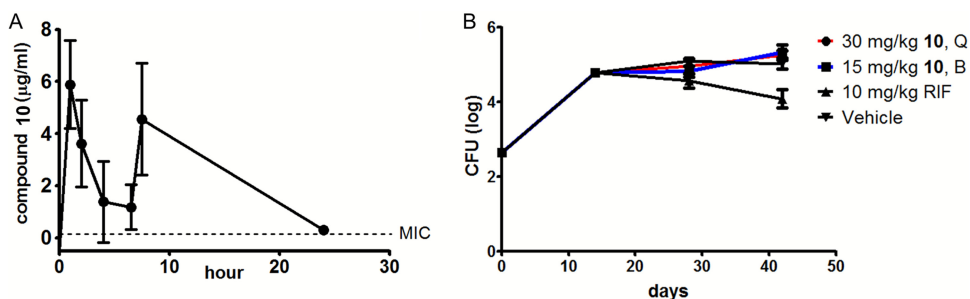


FIG 4 The pyrimidinetrione amide lacks *in vivo* efficacy. (A) PK profile of compound 10 after twice-daily administration at 30 mg/kg. (B) *M. tuberculosis* bacterial burdens in infected mice after 2 and 4 weeks of once-daily or twice-daily treatment at 30 and 15 mg/kg, respectively. Treatment was initiated at 2 weeks after aerosol infection of the mice. The error bars indicate SD. Q, once daily; B, twice daily.

dissociation, with the resultant channel opening driven by this gating mechanism. In line with a loss of regulation of the pore opening of the cation channel, the *corA*::E212D and *corA*::A317 mutants required a 250-fold higher Mg^{2+} concentration in the medium than parental wild-type cells for growth (results not shown). During the preparation of this article, a report was published that found mutations in CorA similar to those of a pyrimidinetrione, as well as a 4-hydroxyquinoline scaffold (19). These mutations were predicted to result in channel opening, resulting in increased cytosolic Mg^{2+} concentrations. Similar to our work, cytosolic concentrations of both free and bound Mg^{2+} decreased, complementing our data showing that these inhibitors directly influence the influx/efflux of the cation.

The observation that the metabolic consequences of CorA inhibition are both growth arrest and death was surprising, since there is an alternative Mg^{2+} transporter encoded by *mgtE* in the bacterium. The finding that mutations in only *corA* could confer resistance suggests that regulation of Mg^{2+} homeostasis by the cation is predominantly conferred by the CorA transporter, where changes in MgtE levels do not occur rapidly enough to overcome this dysregulation of Mg^{2+} homeostasis. In contrast, during genetic inactivation of *corA*, compensatory genetic changes could occur to alter levels of MgtE as cells are gradually depleted of CorA protein. The finding that *corA*, but not *mgtC* or *mgtE*, is conserved in *Mycobacterium leprae*, a mycobacterium with a minimal genome, points to the conserved nature of Mg^{2+} homeostasis by the transporter. Despite this, there is no evidence for the *in vivo* essentiality of *M. tuberculosis corA* during mouse pathogenesis (20). Intriguingly, these compounds were active only against the Gram-positive bacteria tested and not Gram-negative bacteria. CorA is widely distributed in bacteria, including *E. coli* and *P. aeruginosa* (6). Lack of activity against these Gram-negative microbes could be due to lack of binding to their CorA counterpart, different mechanisms of Mg^{2+} homeostasis, lack of transport of the pyrimidinetrione amides across the outer membrane, or their efflux by multidrug efflux pumps.

Our results emphasize the importance of Mg^{2+} homeostasis during active replication, as well as nonreplicating persistence *in vitro* and also during parasitism of host macrophages. Free Mg^{2+} concentrations in the lung were determined to be 0.67 ± 0.08 mM (data not shown), a value similar to reported concentrations in plasma (21), which is below the level that overcomes the growth inhibition by the pyrimidinetrione amides. The lack of *in vivo* efficacy was disappointing, although the pharmacokinetic studies suggested that blood serum drug concentrations were only sufficiently above the MIC for half of the dosing period when extrapolated from the PK parameters (Fig. 4A). Furthermore, the concentration of compound in the cellular lesions may be well below the MIC level during this dosing period. In addition, despite the lack of cytotoxicity of the compound, clinical signs of toxicity were evident when mice were dosed at 100 mg/kg (results not shown), prohibiting additional studies to probe the *in vivo* efficacy of the compound.

In conclusion, our results demonstrate the critical role of CorA in maintaining Mg^{2+} homeostasis and its attractiveness as a drug target. Despite the *in vitro* and *ex vivo* efficacy of the pyrimidinetrione amides, our data suggest that an alternative scaffold that inhibits CorA function would need to be identified in order to perform the proof of concept experiments that establish the validity of this target *in vivo*.

MATERIALS AND METHODS

Chemistry. All chemicals and reagents were purchased from Aldrich (Sigma-Aldrich, St. Louis, MO, USA) and Lancaster (Alfa Aesar, Johnson Matthey Company, Ward Hill, MA, USA) and were used without further purification. Commercially available analogues of pyrimidinetrione amide were purchased from Enamine LLC (Monmouth Junction, NJ, USA), Bionet America, Inc. (Tustin, CA, USA), and MicroCombiChem GmbH (Wiesbaden, Germany). Reactions were monitored by thin-layer chromatography (TLC) performed on silica gel glass plates containing 60 GF-254 (Millipore Sigma, MO, USA), and visualization on TLC was achieved by UV light or iodine indicator. Column chromatography was performed with Merck 60- to 120-mesh silica gel. 1H nuclear magnetic resonance (NMR) spectra were recorded on a Varian Mercury-300 NMR spectrometer, and chemical shifts are reported in parts per million downfield from an internal trimethylsilane (TMS) standard. Routine mass analyses (low-resolution mass spectrometry [LRMS]) were

performed on an HP Agilent liquid chromatography-mass spectrometry (LC-MS) series 1100 system equipped with a reverse-phase column (Agilent Poroshell 120 EC-C18; 2.7 μ m; 50 by 2.1 mm) and a photodiode array detector using electrospray ionization (ESI). All the reported compounds were pure and >95%.

Synthesis of compounds 12 and 14 to 20 (22). To a solution of 1,3-dimethylpyrimidine-2,4,6-(1*H*,3*H*,5*H*)-trione (1.0 eq) in dichloromethane (DCM) (0.1 M) were added pyridine (1.2 eq) and 4-dimethylaminopyridine (0.1 eq) at 0°C. Ethylcarbonochloridate (1.0 eq) was added dropwise to the reaction mixture at the same temperature over 1 h. After stirring for 12 h at 0°C, the reaction mixture was allowed to warm to room temperature and then diluted with DCM and washed with water. The organic layer was dried over Na₂SO₄ and evaporated *in vacuo*. The crude mixture was recrystallized from ethanol to get ethyl 1,3-dimethyl-2,4,6-trioxohexahydropyrimidine-5-carboxylate as a white solid (1.09 g; 75%). ¹H NMR (DMSO [*d*imethyl sulfoxide]-*d*₆, 300 MHz) δ 4.28 (qt, *J* = 6.9 Hz, 2-H), 3.16 (s, 3-H), 1.27 to 1.23 (t, *J* = 6.9 Hz, 3-H); LCMS (ESI) *m/z* 229 [M + H]⁺.

To a solution of ethyl 1,3-dimethyl-2,4,6-trioxohexahydropyrimidine-5-carboxylate (1.0 eq) in toluene (0.5 M) was added each amine (1.0 eq) and triethylamine (TEA) (1.2 eq). The reaction mixture was refluxed for about 12 h. After cooling down to room temperature, the reaction mixture was diluted with ethyl acetate and then washed with water. The organic layer was dried over Na₂SO₄ and evaporated *in vacuo*. The crude mixture was recrystallized from acetonitrile to get the desired products, compounds 12 and 14 to 20.

(i) 1,3-Dimethyl-2,4,6-trioxo-N-(4-phenoxyphenyl)hexahydropyrimidine-5-carboxamide (compound 12). White solid (75%): ¹H NMR (CDCl₃, 300 MHz) δ 11.92 (s, 1-H), 7.46 (d, *J* = 6.9 Hz, 2-H), 7.35 (t, *J* = 7.2 Hz, 2-H), 7.12 (t, *J* = 7.5 Hz, 1-H), 7.03 to 7.00 (m, 4-H), 3.41 (s, 3-H), 3.38 (s, 3-H); LC-MS (ESI) *m/z* 368 [M + H]⁺.

(ii) N-(4-acetylphenyl)-1,3-dimethyl-2,4,6-trioxohexahydropyrimidine-5-carboxamide (compound 14). White solid (79%): ¹H NMR (CDCl₃, 300 MHz) δ 12.10 (s, 1-H), 7.97 (d, *J* = 8.7 Hz, 2-H), 7.63 (d, *J* = 8.7 Hz, 2-H), 3.41 (s, 3-H), 3.37 (s, 3-H), 2.59 (s, 3-H); LC-MS (ESI) *m/z* 318 [M + H]⁺.

(iii) N-(4-bromo-2-fluorophenyl)-1,3-dimethyl-2,4,6-trioxohexahydropyrimidine-5-carboxamide (compound 15). White solid (46%): ¹H NMR (CDCl₃, 300 MHz) δ 12.04 (s, 1-H), 7.98 (t, *J* = 8.5 Hz, 1-H), 7.38 to 7.26 (m, 2-H), 3.42 (s, 3-H), 3.38 (s, 3-H); LC-MS (ESI) *m/z* 370 [M - H]⁻.

(iv) 1,3-Dimethyl-2,4,6-trioxo-N-(2,4,6-trichlorophenyl)hexahydropyrimidine-5-carboxamide (compound 16). White solid (48%): ¹H NMR (CDCl₃, 300 MHz) δ 11.35 (s, 1-H), 7.44 (s, 2-H), 3.40 (s, 3-H), 3.39 (s, 3-H); LC-MS (ESI) *m/z* 378 [M + H]⁺.

(v) N-(6-chloropyridin-3-yl)-1,3-dimethyl-2,4,6-trioxohexahydropyrimidine-5-carboxamide (compound 17). White solid (88%): ¹H NMR (CDCl₃, 300 MHz) δ 11.94 (s, 1-H), 8.52 (d, *J* = 2.4 Hz, 1-H) 8.01 to 7.96 (dd, *J* = 2.7 and 8.7 Hz, 1-H), 7.35 (d, *J* = 8.4 Hz, 1-H), 3.41 (s, 3-H), 3.37 (s, 3-H); LC-MS (ESI) *m/z* 311 [M + H]⁺.

(vi) 1,3-dimethyl-N-(6-methylpyridin-2-yl)-2,4,6-trioxohexahydropyrimidine-5-carboxamide (compound 18). White solid (71%): ¹H NMR (CDCl₃, 300 MHz) δ 12.13 (s, 1-H), 7.70 (d, *J* = 7 Hz, 1-H), 7.63 (t, *J* = 7.8 Hz, 1-H), 6.98 (d, *J* = 7.5 Hz, 1-H), 3.39 (s, 6-H), 2.50 (s, 3-H); LC-MS (ESI) *m/z* 291 [M + H]⁺.

(vii) 1,3-Dimethyl-2,4,6-trioxo-N-(4(trifluoromethyl)pyridin-2-yl)hexahydropyrimidine-5-carboxamide (compound 19). White solid (73%): ¹H NMR (CDCl₃, 300 MHz) δ 12.18 (s, 1-H), 8.55 (d, *J* = 5.1 Hz, 1-H), 8.27 (s, 1-H), 7.32 (d, *J* = 4.8 Hz, 1-H), 3.43 (s, 3-H), 3.39 (s, 3-H); LC-MS (ESI) *m/z* 345 [M + H]⁺.

(viii) 1,3-Dimethyl-N-(5-methylisoxazol-3-yl)-2,4,6-trioxohexahydropyrimidine-5-carboxamide (compound 20). White solid (69%): ¹H NMR (CDCl₃, 300 MHz) δ 12.04 (s, 1-H), 6.52 (s, 1-H), 3.41 (s, 3-H), 3.36 (s, 3-H), 2.43 (s, 3-H); ¹³C NMR (CDCl₃, 75 MHz) δ 169.1, 167.8, 162.8, 161.7, 158.4, 91.7, 81.6, 28.5, 12.1; LC-MS (ESI) *m/z* 281 [M + H]⁺.

Strains, media, and materials. *M. tuberculosis* H37Rv (ATCC 27294) was used for all experiments. To determine the antimicrobial spectrum of the compounds, *B. subtilis* and *S. aureus* were used as Gram-positive strains and *E. coli* and *P. aeruginosa* were used as Gram-negative strains. For liquid cultures, *M. tuberculosis* was grown in 7H9 medium, which consists of Middlebrook 7H9 (Becton, Dickinson) broth base supplemented with albumin (50 g/liter)-dextrose (20 g/liter)-NaCl (8.1 g/liter) (ADC), 0.2% glycerol, and 0.05% Tween 80. Solid agar medium (7H11-OADC) for *M. tuberculosis* growth consisted of Middlebrook 7H11 (Becton, Dickinson) agar base supplemented with OADC (ADC with 0.06% oleic acid). GAST was used as a defined minimal liquid growth medium for *M. tuberculosis* (23). Mg²⁺-free GAST medium was made by omitting MgCl₂·6H₂O from the medium composition. The low-pH nitrosative-stress medium contained bovine serum albumin fraction V (5 g/liter), butyric acid (2.5 mM), NaNO₂ (6.9 mg/ml), NaCl (0.81 g/liter), and 0.05% tyloxapol pH adjusted to 6.0. MIC determination was performed as previously described (23). Luria-Bertani (LB) broth (Difco) was used to determine the MICs of Gram-positive and -negative strains. The screening conditions under which the original pyrimidinetrione hits were identified have been described previously; in brief, they consisted of 7H9 medium with readout of *M. tuberculosis* growth after 3 days of compound exposure (24).

Generation and characterization of pyrimidinetrione-resistant mutants. To generate mutants spontaneously resistant to the compounds, 50 ml of *M. tuberculosis* was grown to an optical density at 650 nm (OD₆₅₀) of 0.2. Harvested cells were resuspended in 500 μ l of medium, and 100- μ l aliquots (10⁹ cells) were plated on 7H11-OADC containing compound 1 at concentrations corresponding to 5 \times , 10 \times , and 20 \times MIC. Appropriate dilutions of the cell suspensions were also plated on drug-free plates to calculate bacterial numbers in the suspensions for determination of frequencies (the resistance frequency is the number of resistant mutants obtained divided by the number of bacteria plated). The agar plates were incubated at 37°C for 4 weeks. After 4 weeks, 4 colonies growing on 7H11-OADC containing 10 \times MIC of compound 1 were inoculated in 7H9 medium, and resistance was confirmed by MIC determination. Genomic DNA of the mutants was isolated by the CTAB (cetyltrimethylammonium

bromide) method (25). Whole-genome sequencing was performed and analyzed as described previously (26).

Cytotoxicity in HepG2 cells. Cytotoxicity in HepG2 cells was measured by CellTiter-Glo luminescent cell viability assay (Promega). For glucose medium, 20,000 HepG2 cells were seeded in 96-well white flat-bottom plates (Corning Inc.) in Dulbecco's modified Eagle's medium (DMEM) GlutaMax (Gibco) supplemented with 10% fetal bovine serum, 20 mM HEPES, and 0.5 mM sodium pyruvate. For galactose medium, HepG2 cells were precultured in galactose DMEM and seeded in the same plate with glucose medium. Galactose DMEM consists of glucose-free DMEM (Gibco) supplemented with 10% fetal bovine serum, 10 mM D-galactose, 2 mM L-glutamine, 5 mM HEPES, and 0.5 mM sodium pyruvate. The plates were incubated at 37°C with 5% CO₂. The following day, 2-fold serial dilutions of compound up to 100 μM were added to the respective growth medium in duplicate, and the cells were incubated for 24 h. After this, 20 μl of CellTiter-Glo reagent was added to each well, followed by incubation at 37°C with 5% CO₂ for 10 min. Cytotoxicity was determined by measuring the luminescence using Fluostar Optima FL (BMG Labtech).

In silico analysis. The amino acid sequence of MtCorA (Rv1239c) was retrieved from the Mycobrowser database (<https://mycobrowser.epfl.ch/>). The FASTA format of the MtCorA protein sequence was submitted to the PHYRE2 protein fold recognition server, and 99 sequence alignment hits were obtained. The sequence of TmCorA was selected as the single highest-scoring template, and 332 residues (91% of the MtCorA sequence) were modeled with 100% confidence by the structure of TmCorA.

Magnesium and cobalt concentration-dependent MIC. We used Mg²⁺-free GAST medium to test the magnesium dependence of the MICs of the compounds. Two-fold-concentrated GAST generated without the addition of magnesium chloride hexahydrate was prepared. An equal volume of magnesium chloride in sterile distilled water was added to the GAST medium to give final concentrations ranging from 0.12 mM up to 240 mM. MIC determinations for the compounds were set up in duplicate as previously described for each MgCl₂ concentration (27). Briefly, 50-μl aliquots of GAST medium at the defined MgCl₂ concentration with compound serially diluted in duplicate from 50 to 0.024 μM were added to all wells of a round-bottom 96-well plate (Nunclon). *M. tuberculosis* culture in GAST at an OD₆₅₀ of 0.2 was diluted 1:500 in 2× Mg²⁺-free GAST, and 50 μl was added to each well of the 96-well plates. The plates were incubated under 5% CO₂ at 37°C. Growth was measured using an inverted enlarging mirror at 1, 2, and 3 weeks, with the MIC taken to be the concentration that completely inhibited all visible growth. For the cobalt-dependent MIC test, CoCl₂ was added to GAST medium at concentrations from 0.001 to 5 mM, and MICs were determined as described above.

Magnesium concentration measurement by ICP-MS. We measured magnesium concentrations in *M. tuberculosis* cells treated by ICP-MS. Two liters of *M. tuberculosis* was grown to an OD₆₅₀ of 0.6 in 7H9. Five hundred-milliliter culture volumes were incubated with 1× and 10× MIC of compound 10, 10× MIC of moxifloxacin, or an equivalent volume of DMSO vehicle control (0.1% [vol/vol]) for 24 h in 2-liter-capacity rolling bottles. Cells were harvested and washed three times with 1/10 volume phosphate-buffered saline containing 0.05% Tween 80 (PBST). The wet weight of *M. tuberculosis* cell pellets was recorded to normalize the magnesium concentration prior to autoclaving. ICP-MS analysis service was provided by Elementary Analysis Inc. (Lexington, KY, USA).

UV spectrum scanning to test magnesium binding of pyrimidinetrione. One milliliter of 100 μM compound 10 dissolved in 100 mM HEPES buffer was put in 1-cm-path-length quartz crystal cuvettes for UV scanning. The absorbance of the compound 10 solution was scanned at 200-nm to 400-nm wavelengths with a Varian Cary 300 Bio UV-Vis spectrophotometer. We sequentially added 10 μl of 1 mM MgSO₄ to the compound solution to observe changes in the absorbance spectrum. A standard curve was plotted with A_{280nm} of 5, 10, 50, and 100 μM compound 10. Absorbance at 280 nm was used to calculate the concentration of compound 10 after correcting for changes in volume, and the values were plotted in a graph.

Minimum magnesium requirement test. *M. tuberculosis* H37Rv, *corA*::E21D, and *corA*::A317S strains were cultured in GAST to an OD₆₅₀ of 0.2 at 37°C. Fifty microliters of Mg²⁺-free GAST was distributed to every well of a round-bottom 96-well plate (Nunclon). Fifty microliters of 240 mM MgCl₂ dissolved in Mg²⁺-free GAST was added to the wells of the first column of the plate, and 50-μl volumes were transferred from column 1 to column 12, generating a 2-fold serial dilution series of MgCl₂ across the plate. *M. tuberculosis* cultures were diluted 1:500 in Mg²⁺-free GAST, and 50 μl was added to each well of the 96-well plates. Growth was measured using an inverted enlarging mirror at 1, 2, and 3 weeks, with the minimum Mg²⁺ concentration to support growth taken to be the lowest concentration that supported any visible evidence of growth.

Cloning, expression, and purification of MtCorA. The *M. tuberculosis corA* gene (*rv1239c*), was cloned into the pET28a vector. The gene was amplified by PCR using Herculase II Fusion DNA polymerase (Agilent) and the following primers: forward, 5'-CGCGGCAGCCATATGTTCCAGGGTTT-3', and reverse, 5'-TGCGGCGCAAGCTTCTAGAGCCAGTTTCT-3'. The PCR-amplified gene was inserted between two restriction sites, NdeI and HindIII, using In-Fusion HD Cloning Plus (TaKaRa). Site-directed mutagenesis was performed to generate the E212D mutation on *corA*. MtCorA contained an N-terminal polyhistidine tag. The plasmids carrying the wild-type and mutant *corA* genes were transformed into OverExpress C41 (DE3) (Lucigen). The cells were grown in LB medium at 37°C. The induction was initiated with 1 mM IPTG (isopropyl-β-D-thiogalactopyranoside) at an OD₆₀₀ of 0.7 to 0.8, and after 6 h, the cells were harvested by centrifugation at 3,500 rpm for 20 min. The cell pellet was resuspended in lysis buffer containing 50 mM Tris-HCl, pH 8.0, 150 mM NaCl, 0.5 mM dithiothreitol (DTT), and SigmaFast protease inhibitor cocktail tablets, EDTA free (Sigma-Aldrich). After sonication, the lysed cells were pelleted by centrifugation at 20,000 × g for 60 min, and the membrane was isolated from the supernatant by ultracentrifugation at

142,000 $\times g$ for 60 min. The isolated membrane was then solubilized in resuspension buffer, 50 mM Tris-HCl, pH 8.0, 300 mM NaCl, 20 mM imidazole, 0.5 mM DTT, with 1% (wt/vol) dodecyl maltoside (DDM) (Anatrace). The resulting supernatant was loaded onto a Ni-nitrilotriacetic acid (NTA) column. The column was washed with wash buffer consisting of 50 mM Tris-HCl, pH 8.0, 300 mM NaCl, 40 mM imidazole, 0.5 mM DTT, with 0.1% (wt/vol) DDM. The CorA or CorA mutant protein was eluted with elution buffer (50 mM Tris-HCl, pH 8.0, 300 mM NaCl, 300 mM imidazole, 0.5 mM DTT, with 0.05% [wt/vol] DDM), and the resulting supernatant fractions containing CorA were identified using SDS-PAGE, pooled, and dialyzed against dialysis buffer (50 mM Tris-HCl, pH 8.0, 100 mM NaCl, 0.5 mM DTT, with 0.05% [wt/vol] DDM). The protein was finally purified on a Superdex 200 16/60 (GE Healthcare) in 50 mM Tris-HCl, pH 8.0, 300 mM NaCl, 0.5 mM DTT, with 0.05% (wt/vol) DDM.

Thermostability test of CorA with pyrimidinetriones. Purified MtCorA samples were diluted to a concentration of 0.5 mg/ml. The solution was aliquoted into 30- μ l volumes, with 1 μ l of a stock solution of different Mg²⁺ concentrations added to the aliquot. Samples were incubated for 20 min at room temperature and then further incubated for 10 min at every increment of 5°C up to 95°C in a thermocycler. The samples were transferred to a 96-well filter plate (0.45 μ m; Millipore) to remove precipitated proteins. The yield of the filtered protein was analyzed by SDS-PAGE.

Substrate binding measured by fluorescence quenching. The dissociation constants between CorA and its ligands, Mg²⁺, Co²⁺, and compound 10, were determined by a ligand dose-dependent fluorescence-quenching assay (Cary Varian Eclipse fluorescence spectrophotometer). CorA was titrated with increasing concentrations of ligands, and fluorescence emission was measured at \sim 350 nm following excitation at 283 nm (bandwidths, 5 nm). The fluorescence quenching (ΔF) versus ligand concentration ($[S]$) was plotted, and the K_d (app) (the apparent dissociation constant of CorA to ligands) values were calculated by fitting the data to an equation, $\Delta F = (F_0 - F) = (\Delta F_{\max} \times [S]) / (K_d(\text{app}) + [S])$, where F_0 and F are the fluorescence intensities in the absence and presence of substrates, respectively.

Efficacy study *in vitro*, *ex vivo*, and *in vivo*. The *in vitro* efficacies of the compounds against *M. tuberculosis* were measured during aerobic growth, as well as during anaerobic, nonreplicating persistence. Time-kill kinetics were measured under aerobic conditions as follows. Logarithmically growing *M. tuberculosis* (OD₆₅₀ = 0.2) was diluted 1,000-fold in 7H9 medium, and 1-ml volumes were exposed to 1 \times , 2 \times , 5 \times , 10 \times , and 20 \times MIC of compound 10 for up to 7 days in duplicate. Samples were collected and plated on 7H11-OADC plates for CFU enumeration at 1, 2, 4, and 7 days of treatment. For anaerobic conditions, *M. tuberculosis* was cultured in the self-generated oxygen depletion model as previously described (27). One-milliliter volumes of anaerobic *M. tuberculosis* culture were exposed for 1 week to 1 \times , 5 \times , 10 \times , 20 \times , and 50 \times MICs of compounds 9, 10, and 20 in an anaerobic chamber (Microbiology International), followed by CFU enumeration as described above.

For *ex vivo* efficacy testing, J774 cells (6.6×10^4 cells/well) were seeded in flat-bottom 24-well plates (Corning Inc.) in J774 growth medium consisting of DMEM GlutaMax (Gibco) supplemented with 10% fetal bovine serum, 20 mM HEPES, and 0.5 mM sodium pyruvate. *M. tuberculosis* H37Rv with confirmed high levels of phthiocerol dimycocerosate was grown in 7H9 to an OD₆₅₀ of 0.5 and filtered through a 5- μ m sterile filter to ensure a single-cell suspension, cell density was confirmed at OD₆₅₀, and the suspension was diluted in J774 growth medium to 4.4×10^5 CFU/ml. Aliquots of 0.1 ml of the *M. tuberculosis* suspension were added to each well of the 24-well plate, giving a multiplicity of infection (MOI) of 1:1.5. After overnight incubation, the medium was aspirated and monolayers were washed twice in prewarmed PBS (pH 7.4) twice. At this point, four wells were used for CFU enumeration as described below. To each of the remaining wells, 1 ml J774 growth medium containing compound or vehicle (DMSO) control was added. Each compound was tested at 1 \times , 5 \times , and 10 \times its MIC in duplicate wells for each time point and concentration. Rifampin (0.5 and 5 μ g/ml) was used as a positive control. Cells were incubated at 37°C, 95% humidity, 5% CO₂ for 3 and 7 days. The medium was replenished at days 3 and 5, taking care not to remove any macrophages, since the pyrimidinetrione amides resulted in loss of adherence of macrophages over time. After 3 or 7 days of incubation, medium was removed, taking care not to remove macrophages, and 1 ml of 7H9 medium containing 0.1% SDS was added to each well to ensure macrophage lysis. After 5 min, the lysate was rapidly mixed to shear eukaryotic DNA, diluted in 7H9, and plated on 7H11-OADC plates. Colonies were enumerated after 4 weeks of incubation at 37°C.

Mouse studies were carried out in accordance with the Guide for the Care and Use of Laboratory Animals of the National Institutes of Health under animal study protocol number LCIM 4E. Pharmacokinetic analyses on 20 C57BL/6J mice were done by administering 30 mg/kg compound 10 suspended in 10% (2-hydroxypropyl)- β -cyclodextrin with 50 mM tricine (pH 8.2) twice per day (with a separation of 7 h) by oral gavage, followed by blood sampling at 0.5, 1, 2, 4, 8, 12, and 24 h; 0.1 ml of blood was collected twice from each animal during the experiment in Li-Heparin Microvette tubes (Sarstedt AG & Co., Numbrecht, Germany) and centrifuged to prepare plasma. The tolerability of compound 10 was tested by dosing 5 naive mice twice per day with 100 or 30 mg/kg for 7 days with observation for 7 subsequent days. For evaluation of *in vivo* efficacy, C57BL/6J mice were infected by the aerosol route, as previously described (28). After 14 days, groups of 10 mice were dosed with compound 10 given by oral gavage of either 15 mg/kg or 30 mg/kg twice a day. The higher-dose group developed signs of distress after 1 week, so the dose to that group was de-escalated to 30 mg/kg once a day. Control groups were dosed with vehicle control [10% (2-hydroxypropyl)- β -cyclodextrin] with 50 mM tricine (pH 8.2) or 10 mg/kg rifampin. After 2 and 4 weeks of treatment, groups of 5 mice were euthanized, and appropriate dilutions in 7H9 medium of lung and spleen homogenates were plated on 7H11-OADC plates for CFU enumeration.

Pharmacokinetic analysis of pyrimidinetriones. Pharmacokinetic plasma samples were analyzed with an Agilent 1200 Infinity high-performance liquid chromatography (HPLC) instrument with an Agilent

6460C triple-quadrupole mass selective detector (LC-QqQ) utilizing ESI. Samples were prepared by mixing 50 μ l serum with 50 μ l labetalol internal standard (IS), 20 μ l water, or spike solution, followed by 400 μ l acetonitrile-methanol (3:1) for protein precipitation. Samples were centrifuged at 13,000 rpm for 5 min, and 5 μ l supernatant was injected into a 2.1- by 50-mm Eclipse Plus C₁₈ 1.8- μ m column utilizing 0.1% formic acid in water (solvent A) and acetonitrile with 0.1% formic acid (solvent B). The solvent gradient program was as follows: 8% B, hold for 0.5 min, increase to 95% B in 4.5 min, with a flow rate of 0.8 ml/min.

Multiple reaction monitoring (MRM) transition for compound 10 was detected as [M – H][–] precursor (Q1), collision energy voltage (CEV) 24 V, and 155 product ion (Q2) negative mode, and IS was detected as [M + H]⁺ precursor (Q1), CEV 8V, and 311.2 product ion (Q2) positive mode. PK parameters were calculated using PK macros in Excel.

SUPPLEMENTAL MATERIAL

Supplemental material for this article may be found at <https://doi.org/10.1128/AAC.01006-19>.

SUPPLEMENTAL FILE 1, PDF file, 0.4 MB.

ACKNOWLEDGMENTS

This work was funded in part by the Intramural Research Program of NIAID (AI000693-25) and by grants from the Foundation for the National Institutes of Health (BARRY11HTB0) with support from the Bill and Melinda Gates Foundation (OPP1024021). The funders had no role in study design, data collection and interpretation, or the decision to submit the work for publication.

We gratefully acknowledge the assistance of Danielle Weiner in animal efficacy experiments and Aashish Srivastava for preparing samples for sequencing.

REFERENCES

- Leung CC, Lange C, Zhang Y. 2013. Tuberculosis: current state of knowledge: an epilogue. *Respirology* 18:1047–1055. <https://doi.org/10.1111/resp.12156>.
- Horsburgh CR, Jr, Barry CE, III, Lange C. 2015. Treatment of tuberculosis. *N Engl J Med* 373:2149–2160. <https://doi.org/10.1056/NEJMra1413919>.
- Barry CE. 2011. Lessons from seven decades of antituberculosis drug discovery. *Curr Top Med Chem* 11:1216–1225. <https://doi.org/10.2174/156802611795429158>.
- Gopal P, Dick T. 2014. Reactive dirty fragments: implications for tuberculosis drug discovery. *Curr Opin Microbiol* 21:7–12. <https://doi.org/10.1016/j.mib.2014.06.015>.
- Libardo JMD, Boshoff HI, Barry CE III, 2018. The present state of the tuberculosis drug development pipeline. *Curr Opin Pharmacol* 42:81–94. <https://doi.org/10.1016/j.coph.2018.08.001>.
- Maguire ME. 2006. Magnesium transporters: properties, regulation and structure. *Front Biosci* 11:3149–3163. <https://doi.org/10.2741/2039>.
- Groisman EA, Hollands K, Kriner MA, Lee EJ, Park SY, Pontes MH. 2013. Bacterial Mg²⁺ homeostasis, transport, and virulence. *Annu Rev Genet* 47:625–646. <https://doi.org/10.1146/annurev-genet-051313-051025>.
- Buchmeier N, Blanc-Potard A, Ehrst S, Piddington D, Riley L, Groisman EA. 2000. A parallel intraphagosomal survival strategy shared by *Mycobacterium tuberculosis* and *Salmonella enterica*. *Mol Microbiol* 35:1375–1382. <https://doi.org/10.1046/j.1365-2958.2000.01797.x>.
- Goodsmith N, Guo XV, Vandal OH, Vaubourgeix J, Wang R, Botella H, Song S, Bhatt K, Liba A, Salgame P, Schnappinger D, Ehrst S. 2015. Disruption of an *M. tuberculosis* membrane protein causes a magnesium-dependent cell division defect and failure to persist in mice. *PLoS Pathog* 11:e1004645. <https://doi.org/10.1371/journal.ppat.1004645>.
- Walters SB, Dubnau E, Kolesnikova I, Laval F, Daffe M, Smith I. 2006. The *Mycobacterium tuberculosis* PhoPR two-component system regulates genes essential for virulence and complex lipid biosynthesis. *Mol Microbiol* 60:312–330. <https://doi.org/10.1111/j.1365-2958.2006.05102.x>.
- Garcia-del Portillo F, Foster JW, Maguire ME, Finlay BB. 1992. Characterization of the micro-environment of *Salmonella typhimurium*-containing vacuoles within MDCK epithelial cells. *Mol Microbiol* 6:3289–3297. <https://doi.org/10.1111/j.1365-2958.1992.tb02197.x>.
- Piddington DL, Kashkouli A, Buchmeier NA. 2000. Growth of *Mycobacterium tuberculosis* in a defined medium is very restricted by acid pH and Mg(2+) levels. *Infect Immun* 68:4518–4522. <https://doi.org/10.1128/IAI.68.8.4518-4522.2000>.
- Sassetti CM, Boyd DH, Rubin EJ. 2003. Genes required for mycobacterial growth defined by high density mutagenesis. *Mol Microbiol* 48:77–84. <https://doi.org/10.1046/j.1365-2958.2003.03425.x>.
- Lamichhane G, Zignol M, Blades NJ, Geiman DE, Dougherty A, Grosset J, Broman KW, Bishai WR. 2003. A postgenomic method for predicting essential genes at subsaturation levels of mutagenesis: application to *Mycobacterium tuberculosis*. *Proc Natl Acad Sci U S A* 100:7213–7218. <https://doi.org/10.1073/pnas.1231432100>.
- Anderson CM, Norquist BA, Vesce S, Nicholls DG, Soine WH, Duan S, Swanson RA. 2002. Barbiturates induce mitochondrial depolarization and potentiate excitotoxic neuronal death. *J Neurosci* 22:9203–9209. <https://doi.org/10.1523/JNEUROSCI.22-21-09203.2002>.
- Marroquin LD, Hynes J, Dykens JA, Jamieson JD, Will Y. 2007. Circumventing the Crabtree effect: replacing media glucose with galactose increases susceptibility of HepG2 cells to mitochondrial toxicants. *Toxicol Sci* 97:539–547. <https://doi.org/10.1093/toxsci/kfm052>.
- Kelley LA, Mezulis S, Yates CM, Wass MN, Sternberg MJ. 2015. The Phyre2 web portal for protein modeling, prediction and analysis. *Nat Protoc* 10:845–858. <https://doi.org/10.1038/nprot.2015.053>.
- Mouscadet JF, Tchertanov L. 2009. Raltegravir: molecular basis of its mechanism of action. *Eur J Med Res* 14(Suppl 3):5–16. <https://doi.org/10.1186/2047-783x-14-s3-5>.
- Lopez Quezada L, Silve S, Kelinske M, Liba A, Diaz Gonzalez C, Kotev M, Goullieux L, Sans S, Roubert C, Lagrange S, Bacqué E, Couturier C, Pellet A, Blanc I, Ferron M, Debu F, Li K, Aubé J, Roberts J, Little D, Ling Y, Zhang J, Gold B, Nathan C. 2019. Bactericidal disruption of magnesium metallostatics in *Mycobacterium tuberculosis* is counteracted by mutations in the metal ion transporter CorA. *mBio* 10:e01405-19. <https://doi.org/10.1128/mBio.01405-19>.
- Zhang YJ, Reddy MC, Ioerger TR, Rothchild AC, Dartois V, Schuster BM, Trauner A, Wallis D, Galaviz S, Huttenhower C, Sacchetti JC, Behar SM, Rubin EJ. 2013. Tryptophan biosynthesis protects mycobacteria from CD4 T-cell-mediated killing. *Cell* 155:1296–1308. <https://doi.org/10.1016/j.cell.2013.10.045>.
- Laarakker MC, van Lith HA, Ohl F. 2011. Behavioral characterization of A/J and C57BL/6J mice using a multidimensional test: association between blood plasma and brain magnesium-ion concentration with anxiety. *Physiol Behav* 102:205–219. <https://doi.org/10.1016/j.physbeh.2010.10.019>.
- Wang D, Zhang Z, Lu X, Feng Y, Luo K, Gan J, Yingxue L, Wan J, Li X,

- Zhang F, Tu Z, Cai Q, Ren X, Ding K, Ding K. 2011. Hybrid compounds as new Bcr/Abl inhibitors. *Bioorg Med Chem Lett* 21:1965–1968. <https://doi.org/10.1016/j.bmcl.2011.02.029>.
23. Duckworth BP, Wilson DJ, Nelson KM, Boshoff HI, Barry CE, Aldrich CC. 2012. Development of a selective activity-based probe for adenylating enzymes: profiling MbtA involved in siderophore biosynthesis from *Mycobacterium tuberculosis*. *ACS Chem Biol* 7:1653–1658. <https://doi.org/10.1021/cb300112x>.
24. Oh S, Park Y, Engelhart CA, Wallach JB, Schnappinger D, Arora K, Manikkam M, Gac B, Wang H, Murgolo N, Olsen DB, Goodwin M, Sutphin M, Weiner DM, Via LE, Boshoff HIM, Barry CE. 2018. Discovery and structure-activity-relationship study of N-alkyl-5-hydroxypyrimidinone carboxamides as novel antitubercular agents targeting decaprenylphosphoryl-beta-d-ribose 2'-oxidase. *J Med Chem* 61:9952–9965. <https://doi.org/10.1021/acs.jmedchem.8b00883>.
25. Alland D, Steyn AJ, Weisbrod T, Aldrich K, Jacobs WR, Jr. 2000. Characterization of the *Mycobacterium tuberculosis* iniBAC promoter, a promoter that responds to cell wall biosynthesis inhibition. *J Bacteriol* 182:1802–1811. <https://doi.org/10.1128/JB.182.7.1802-1811.2000>.
26. Ioerger TR, Feng Y, Ganesula K, Chen X, Dobos KM, Fortune S, Jacobs WR, Jr, Mizrahi V, Parish T, Rubin E, Sassetti C, Sacchettini JC. 2010. Variation among genome sequences of H37Rv strains of *Mycobacterium tuberculosis* from multiple laboratories. *J Bacteriol* 192:3645–3653. <https://doi.org/10.1128/JB.00166-10>.
27. Park Y, Pacitto A, Bayliss T, Cleghorn LAT, Wang Z, Hartman T, Arora K, Ioerger TR, Sacchettini J, Rizzi M, Donini S, Blundell TL, Ascher DB, Rhee K, Breda A, Zhou N, Dartois V, Jonnala SR, Via LE, Mizrahi V, Epemolu O, Stojanovski L, Simeons F, Osuna-Cabello M, Ellis L, MacKenzie CJ, Smith ARC, Davis SH, Murugesan D, Buchanan KI, Turner PA, Huggett M, Zuccotto F, Rebollo-Lopez MJ, Lafuente-Monasterio MJ, Sanz O, Diaz GS, Lelièvre J, Ballell L, Selenski C, Axtman M, Ghidelli-Disse S, Pflaumer H, Bösche M, Drewes G, Freiberg GM, Kurnick MD, Srikumaran M, Kempf DJ, Green SR, Ray PC, Read K, Wyatt P, Barry CE, Boshoff HI. 2017. Essential but not vulnerable: indazole sulfonamides targeting inosine monophosphate dehydrogenase as potential leads against *Mycobacterium tuberculosis*. *ACS Infect Dis* 3:18–33. <https://doi.org/10.1021/acsinfecdis.6b00103>.
28. Singh R, Barry CE III, Boshoff HI. 2010. The three RelE homologs of *Mycobacterium tuberculosis* have individual, drug-specific effects on bacterial antibiotic tolerance. *J Bacteriol* 192:1279–1291. <https://doi.org/10.1128/JB.01285-09>.